Characterization, Evaluation, and Design of Noise Separator for Conducted EMI Noise Diagnosis

Shuo Wang, *Student Member, IEEE*, Fred. C. Lee, *Fellow, IEEE*, and Willem Gerhardus Odendaal, *Member, IEEE*

***Abstract*—In this paper, at first, three requirements for noise separators are specified and the disadvantages of traditional evaluation methods are pointed out. Noise separators are then characterized using scattering parameters (S-parameters). Existing noise separators are evaluated according to the specified requirements. Finally a noise separator is proposed with parasitic controlled design and the prototype is evaluated using the proposed method. An electromagnetic interference (EMI) measurement shows that the proposed noise separator can effectively separate noise and that it is easy to use.**

***Index Terms*—Common/differential-mode rejection ratio, common/differential-mode transmission ratio, line impedance stabilization network (LISN), noise separator, scattering parameters, transmission line transformer.**

I. Introduction

SEPARATION of conducted differential-mode (DM) and common-mode (CM) noise is very useful for noise diagnosis and electromagnetic interference (EMI) filter design in power electronics applications. Many papers have discussed and proposed noise separators [1]–[9], [16], but few of them seriously characterized, evaluated and designed the separator. As a result, many of these noise separators fail to offer correct or accurate DM and CM noise separation.

For a typical noise measurement setup for a power factor correction (PFC) converter, as shown in Fig. 1, parasitic capacitors, especially the parasitic capacitor C_C between the drain of the MOSFET and the ground, offer paths for CM noise through the heat-sink. The CM noise $2\mathbf{i_{CM}}$ comes back to the converter through 50 Ω terminations and line impedance stabilizing networks (LISNs). DM noise $\mathbf{i_{DM}}$ also flows through LISNs and 50 Ω terminations due to the high impedance of the two 50 μH inductors in the LISNs. Here, 50 Ω terminations can also be the input impedances of a spectrum analyzer. The DM or CM noise voltage drop on a 50 Ω resistance is defined as DM or CM noise voltage.

In Fig. 2, the noise voltage drop $\mathbf{V_1}$ or $\mathbf{V_2}$ on one of the 50 Ω terminations is defined as the total noise, and it is the vector sum or vector difference of CM and DM noise voltages. The DM and CM noise voltages can then be calculated from (1) and (2). In order to separate DM and CM noise, the noise separator should satisfy three requirements.

1) Input impedances are always real 50 Ω and are independent from noise source impedances.

Manuscript received April 13, 2004; revised August 18, 2004. Recommended by Associate Editor F. Blaabjerg.

The authors are with the Bradley Department of Electrical and Computer Engineering, Virginia Polytechnic Institute and State University, Blacksburg, VA 24061 USA (e-mail: shwang6@vt.edu).

Digital Object Identifier 10.1109/TPEL.2005.850978

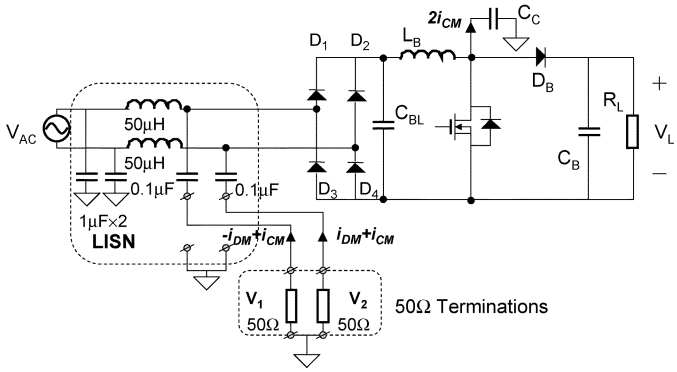

Fig. 1. EMI noise measurement setup for a PFC converter.

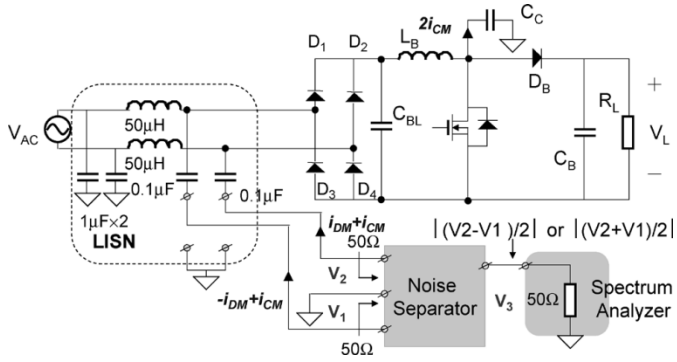

Fig. 2. Using noise separator to separate DM and CM noise.

2) Output is $|(\mathbf{V_1}-\mathbf{V_2})/2|$ for DM noise measurement and $|(\mathbf{V_1}+\mathbf{V_2})/2|$ for CM noise measurement.
3) Leakage between the CM and the DM at the output should be small.

$$|\mathbf{V_{DM}}| = \left|\frac{\mathbf{V_2}-\mathbf{V_1}}{2}\right| = 50|\mathbf{i_{DM}}| \tag{1}$$

$$|\mathbf{V_{CM}}| = \left|\frac{\mathbf{V_2}+\mathbf{V_1}}{2}\right| = 50|\mathbf{i_{CM}}|. \tag{2}$$

The requirement 1) guarantees consistent measurement conditions and accurate sampling of noise voltage, 2) guarantees correct noise separation, and 3) guarantees small interference between the CM and DM noise measurements. Most of the noise separators [1]–[9], [16] cannot satisfy all these three requirements, and therefore measurement results are questionable. For example, input impedances of many separators are noise source dependent. These noise separators do not yield correct measurement results because their input impedances are functions of input voltages or source impedances. Other separators fail to satisfy requirement 2); therefore they lack an accurate output. In

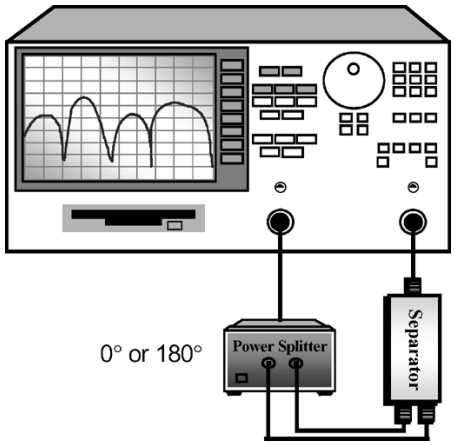

Fig. 3. Using a power splitter and a network analyzer to measure the noise separator may not yield accurate results.

order to evaluate a noise separator, the above three requirements should be checked one by one. The first is input impedance. Papers [3], [4] designed and measured input impedance for one input port, assuming the input of another port was zero with a 50 Ω source impedance; this method is not correct, because another input can affect the input impedance of the designed port and the practical source impedance is not 50 Ω. The second requirement is the transmission coefficient of noise separators. The DM transmission ratio (DMTR) for the DM noise separator and the CM transmission ratio (CMTR) for the CM noise separator are two parameters that need to be evaluated, as

$$\text{For DM noise separator}: DMTR = \left|\frac{\mathbf{V_{OD}}}{\mathbf{V_{DM}}}\right| \tag{3}$$

$$\text{For CM noise separator}: CMTR = \left|\frac{\mathbf{V_{OC}}}{\mathbf{V_{CM}}}\right| \tag{4}$$

where $\mathbf{V_{DM}}$ is the DM voltage fed to the inputs of a DM noise separator, $\mathbf{V_{OD}}$ is the output voltage of this DM noise separator due to $\mathbf{V_{DM}}$, $\mathbf{V_{CM}}$ is the CM voltage fed to the inputs of a CM noise separator, and $\mathbf{V_{OC}}$ is the output voltage of this CM noise separator due to $\mathbf{V_{CM}}$. From (3), (4), the ideal DMTR and CMTR should be 0 dB. Papers [2], [3], [6] used power splitters to generate CM and DM sources and then evaluated the transmission coefficients of the noise separators using a network analyzer, as shown in Fig. 3. This method has three potential problems. First, in point of network analysis, the measured result is only valid when noise source is a power splitter. In fact, nine network parameters are needed to fully characterize a three-port noise separator. The measured transmission coefficient is only one parameter, which does not guarantee the noise separator has the similar performance when noise source is not a power splitter. Second, the power splitter is imperfect, and its negative effects cannot be excluded through calibration of the network analyzer. For example, the phase difference of its two outputs is not exactly 0° or 180°, and this may cause significant measurement errors [5], [9]. The magnitude difference of the two outputs can cause similar problems [5], [9]. Third, for a two-way power splitter, the amplitude of the outputs is 3-dB lower than its input and the network analyzer's reference, so the measured DMTR, CMTR, DMRR and CMRR are 3-dB lower than they should be. The third requirement can be characterized

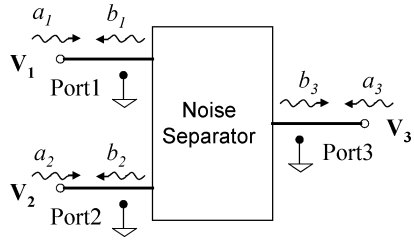

Fig. 4. Characterizing noise separator in terms of waves.

by two parameters: the CM rejection ratio (CMRR) and the DM rejection ratio (DMRR), which are defined as

$$\text{For DM noise separator}: CMRR = \left|\frac{\mathbf{V_{OD}}}{\mathbf{V_{CM}}}\right| \tag{5}$$

$$\text{For CM noise separator}: DMRR = \left|\frac{\mathbf{V_{OC}}}{\mathbf{V_{DM}}}\right| \tag{6}$$

where $\mathbf{V_{CM}}$ is the CM voltage fed to the inputs of a DM noise separator, $\mathbf{V_{OD}}$ is the output voltage of this DM noise separator due to $\mathbf{V_{CM}}$, $\mathbf{V_{DM}}$ is the DM voltage fed to the inputs of a CM noise separator, and $\mathbf{V_{OC}}$ is the output voltage of this CM noise separator due to $\mathbf{V_{DM}}$. CMRR and DMRR should be as small as possible.

For the same reason as the second requirement, if a power splitter is used to evaluate CMRR and DMRR, the measurement does not guarantee the noise separator has the similar performance in practical applications; thus the method is not adequate.

Appropriate network parameters must be introduced in order to characterize and evaluate noise separators using the three requirements. Scattering parameters (S-parameters) are selected in this paper because of three reasons. First, frequency domain characterization of network employing $[\boldsymbol{Z}]$, $[\boldsymbol{Y}]$, $[\boldsymbol{H}]$ and $[\boldsymbol{ABCD}]$ parameters often requires either a short circuit or an open circuit at one port, which is difficult to achieve in the high frequency (HF) range because of parasitic parameters [14], [15]. On the other hand, for S-parameters, no short or open circuit is needed. Second, S-parameter method can be calibrated to the exact points of measurement, so that the effects of parasitics due to measurement interconnects are excluded. For $[\boldsymbol{Z}]$, $[\boldsymbol{Y}]$, $[\boldsymbol{H}]$ and $[\boldsymbol{ABCD}]$ parameters measurement, expensive special probes may be needed for calibration. Third, S-parameters are analytically convenient, and capable of providing a great insight into a measurement or design problem [15]. Thanks to S-parameters, the powerful signal flow graph can be used for network analysis with clear physical concepts.

II. Characterization of Noise Separator

For a DM or CM noise separator, there are two input ports port1 and port2 and one output port port3 so it is a three-port network. This three-port linear passive network can be characterized in terms of waves, as shown in Fig. 4. In Fig. 4, a_n is the normalized incident wave, and b_n is the normalized reflected wave. Port voltage $\mathbf{V_n}$ can be expressed by (7) [10], [11]

$$\mathbf{V_n} = \sqrt{Z_0}(a_n + b_n) \tag{7}$$

where Z_0 is the reference impedance, which is usually 50 Ω, and n is the port number.

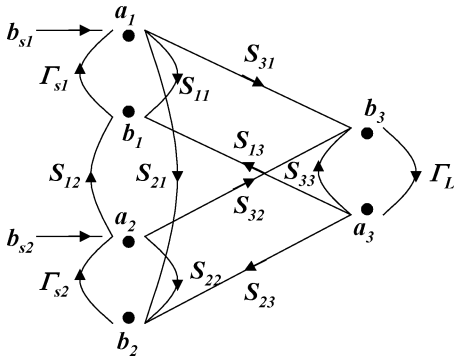

Fig. 5. Characterizing the noise separator using a signal flow graph.

To fully characterize a three-port linear passive network, three linear equations are required among the six wave variables [11]. The nine S-parameters in (8) are therefore introduced to correlate a_n and b_n [10], [12]. S_{nn} refers to the reflection coefficients, and S_{mn} represents the transmission coefficients. According to the transmission-line theory [10], [13], when reflected wave b_n reaches the source or load side, it will also be reflected because of the mismatched impedances. The reflection coefficients Γ_{sn} at source side and Γ_L at load side are given through (9) and (10). It is known that for passive networks, $|\Gamma_{sn}| \leq 1$ and $|\Gamma_L| \leq 1$

$$\begin{pmatrix} b_1 \\ b_2 \\ b_3 \end{pmatrix} = \begin{pmatrix} S_{11} & S_{12} & S_{13} \\ S_{21} & S_{22} & S_{23} \\ S_{31} & S_{32} & S_{33} \end{pmatrix} \begin{pmatrix} a_1 \\ a_2 \\ a_3 \end{pmatrix} \Rightarrow [\mathbf{b}]=[\mathbf{S}][\mathbf{a}] \quad (8)$$

$$\Gamma_{sn}=\frac{Z_{Sn}-Z_0}{Z_{Sn}+Z_0} \quad (9)$$

$$\Gamma_L=\frac{Z_L-Z_0}{Z_L+Z_0}. \quad (10)$$

Fig. 4 is then characterized by the signal flow graph in Fig. 5. In Fig. 5, b_{sn} is the normalized wave emanating from the source. For a given voltage source $\mathbf{V_{sn}}$ with source impedance Z_{sn}, b_{sn} is given by (11) [13]

$$b_{Sn}=\frac{\sqrt{Z_0}\mathbf{V_{Sn}}}{Z_{Sn}+Z_0}. \quad (11)$$

Because the output of the noise separator is terminated by the 50 Ω input impedance of the spectrum analyzer, which is shown in Fig. 2, reflection coefficient Γ_L is zero. As a result, a_3 is zero, and the signal-flow graph is equivalent to Fig. 6. Fig. 6 characterizes a practical noise separator matched by a spectrum analyzer at port3. It is now important to determine the appropriate S matrix for an ideal noise separator.

In order to achieve 50 Ω input impedance independent from noise source impedance, the reflection coefficients at port1 and port2 must be zero. The reflection coefficients Γ_1 and Γ_2 for port1 and port2 in Fig. 6 are described as

$$\Gamma_1=\frac{Z_{in1}-Z_0}{Z_{in1}+Z_0}=S_{11}+\frac{S_{21}\Gamma_{s2}S_{12}}{1-S_{22}\Gamma_{s2}} \quad (12)$$

$$\Gamma_2=\frac{Z_{in2}-Z_0}{Z_{in2}+Z_0}=S_{22}+\frac{S_{21}\Gamma_{s1}S_{12}}{1-S_{11}\Gamma_{s1}} \quad (13)$$

where Z_{in1} and Z_{in2} are the input impedances of port1 and port2. From (12), (13), in order to guarantee a 50-Ω input impedance independent from noise source impedance, S_{11}, S_{22}, and S_{12}, S_{21} must be zero; therefore b_1 and b_2 are zero.

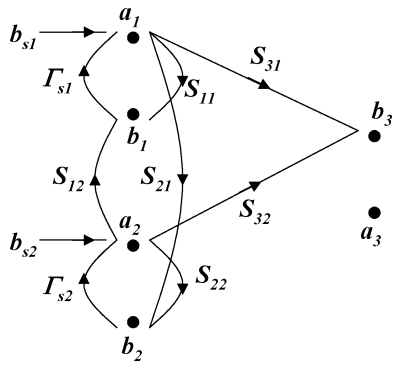

Fig. 6. Signal-flow graph for a practical noise separator with a matched load at port3.

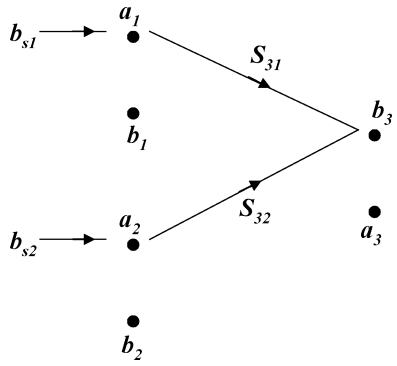

Fig. 7. Signal-flow graph for an ideal noise separator with a matched load at port3.

So the signal-flow graph is thus equivalent to Fig. 7. In Fig. 7, based on (7), the voltage at port3 is given by

$$\mathbf{V_3}=\mathbf{V_1}S_{31}+\mathbf{V_2}S_{32}. \quad (14)$$

Based on (1), (2), (14), for a DM noise separator

$$S_{31}=-S_{32}=\frac{1}{2},\ \text{or}\ -S_{31}=S_{32}=\frac{1}{2}. \quad (15)$$

For a CM noise separator

$$S_{31}=S_{32}=\frac{1}{2},\ \text{or}\ -S_{31}=-S_{32}=\frac{1}{2}. \quad (16)$$

The final $\mathbf{S}$ matrix for an ideal DM noise separator is therefore

$$[\mathbf{S}]=\begin{pmatrix} 0 & 0 & S_{13} \\ 0 & 0 & S_{23} \\ \pm\frac{1}{2} & \mp\frac{1}{2} & S_{33} \end{pmatrix}. \quad (17)$$

And for an ideal CM noise separator

$$[\mathbf{S}]=\begin{pmatrix} 0 & 0 & S_{13} \\ 0 & 0 & S_{23} \\ \pm\frac{1}{2} & \pm\frac{1}{2} & S_{33} \end{pmatrix}. \quad (18)$$

In (17) and (18), the third column in the $\mathbf{S}$ matrix has nothing to do with the performance of a noise separator because port3 is matched. Therefore, there is no need to match output impedance although paper [3] tries to get 50 Ω output impedance. For a noise separator, S_{11}, S_{22} and S_{12}, S_{21} should be as small as possible. S_{31} and S_{32} should be 0.5, and should be out of phase for a DM noise separator, and in phase for a CM noise separator.

For a practical noise separator, S_{11}, S_{22} and S_{12}, S_{21} are not zero; and S_{31} and S_{32} are not exactly 0.5, so Fig. 6 should be

used for evaluation. The input impedance of a noise separator can be evaluated through (12) and (13). In (12) and (13), the second term can be ignored if it is much smaller than the first term, which means input impedances are independent from Γ_{s1} and Γ_{s2}, which represent the source impedances. Then the input impedances can be characterized solely by S_{11} and S_{22}, and are free of noise source impedances

$$Z_{in1} \approx Z_0 \frac{1+S_{11}}{1-S_{11}} \tag{19}$$

$$Z_{in2} \approx Z_0 \frac{1+S_{22}}{1-S_{22}}. \tag{20}$$

Based on (3), (4), (7), and Fig. 6, the DMTR for the DM noise separator and the CMTR for the CM noise separator can also be derived using Mason's rule [see (21) and (22)], in which the approximately equal values hold if the third term is much smaller than the second term in the denominators. This is also the condition for independent real 50 Ω in (19) and (20)

For DM noise separator :

$$DMTR = \frac{S_{31}}{\left(1+S_{11}+\frac{S_{21}\Gamma_{s2}S_{12}}{1-S_{22}\Gamma_{s2}}\right)} - \frac{S_{32}}{\left(1+S_{22}+\frac{S_{21}\Gamma_{s1}S_{12}}{1-S_{11}\Gamma_{s1}}\right)} \approx \frac{S_{31}}{1+S_{11}} - \frac{S_{32}}{1+S_{22}}. \tag{21}$$

For CM noise separator :

$$CMTR = \frac{S_{31}}{\left(1+S_{11}+\frac{S_{21}\Gamma_{s2}S_{12}}{1-S_{22}\Gamma_{s2}}\right)} + \frac{S_{32}}{\left(1+S_{22}+\frac{S_{21}\Gamma_{s1}S_{12}}{1-S_{11}\Gamma_{s1}}\right)} \approx \frac{S_{31}}{1+S_{11}} + \frac{S_{32}}{1+S_{22}}. \tag{22}$$

Based on (5), (6), (7), and Fig. 6, the CMRR for the DM noise separator and the DMRR for the CM noise separator can be derived similarly as follows:

For DM noise separator :

$$CMRR = \frac{S_{31}}{\left(1+S_{11}+\frac{S_{21}\Gamma_{s2}S_{12}}{1-S_{22}\Gamma_{s2}}\right)} + \frac{S_{32}}{\left(1+S_{22}+\frac{S_{21}\Gamma_{s1}S_{12}}{1-S_{11}\Gamma_{s1}}\right)} \approx \frac{S_{31}}{1+S_{11}} + \frac{S_{32}}{1+S_{22}} \tag{23}$$

For CM noise separator :

$$DMRR = \frac{S_{31}}{\left(1+S_{11}+\frac{S_{21}\Gamma_{s2}S_{12}}{1-S_{22}\Gamma_{s2}}\right)} - \frac{S_{32}}{\left(1+S_{22}+\frac{S_{21}\Gamma_{s1}S_{12}}{1-S_{11}\Gamma_{s1}}\right)} \approx \frac{S_{31}}{1+S_{11}} - \frac{S_{32}}{1+S_{22}}. \tag{24}$$

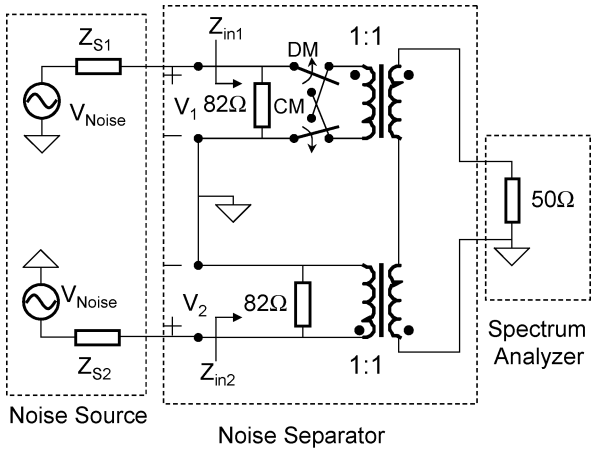

Fig. 8. Noise separator proposed by paper [1].

Equations (19)–(24) are critical for noise-separator evaluation. For a noise separator, as long as the S-parameters are measured using a network analyzer, its performance can be evaluated through (19)–(24). No extra power splitter is needed; therefore the results can be applied to any applications. In (12) and (13), if $S_{21}S_{12}$ is small enough to make the second term approach zero or much smaller than the first term, the input impedances are independent from noise source impedances.

III. Evaluation of Existing Noise Separators

Just as stated in chapter I, a qualified noise separator should meet three requirements. The first requirement is independent real 50-Ω input impedances. Some existing noise separators assume the noise impedances are infinite [1], [2], [5], [9], real 50 Ω [3], [4] or 0 Ω [7]. This is not correct because the noise source impedances can be any value. As an example, the noise separator in paper [1] is shown in Fig. 8. The input impedances for this separator are given as

$$Z_{in1} = 82//(50+82//Z_{S2}), \text{ and} \tag{25}$$

$$Z_{in2} = 82//(50+82//Z_{S1}). \tag{26}$$

Obviously, if $Z_{S1} = Z_{S2} = \infty$, $Z_{in1} = Z_{in2} \approx 50\ \Omega$; however for practical cases, $Z_{S1} \neq \infty$ and $Z_{S2} \neq \infty$, so $Z_{in1} \neq 50\ \Omega$ and $Z_{in2} \neq 50\ \Omega$. This also means the input impedances are functions of the input voltages. As a result, this noise separator cannot correctly separate noise. Theoretically, only the noise separators in papers [6], [16] can offer 50 Ω input impedances.

Under the condition of real 50 Ω input impedances, CMTR and DMTR should be 0 dB, which is the second requirement. Because the noise separators in paper [1]–[5], [7], [9] cannot meet the first requirement, they certainly cannot meet the second one. The input impedances of the noise separator (power combiner) in paper [6] are real 50 Ω; however both CMTR and DMTR are 3 dB higher. Furthermore, two set of circuits are needed to measure CM and DM noise respectively. The noise separator in paper [16], which is shown in Fig. 9, meets 0 dB CMTR but its DMTR is 6 dB higher.

The third requirement is very small CMRR and DMRR. The noise separator works at frequencies as high as 30 MHz, so parasitic parameters play very important roles on separator perfor-

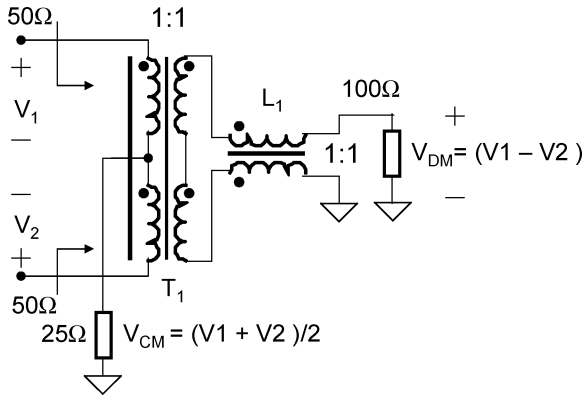

Fig. 9. Noise separator proposed by paper [16].

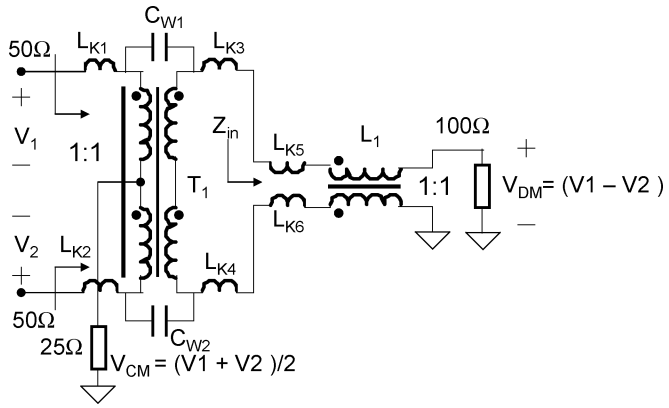

Fig. 10. Parasitic parameters in a noise separator.

mance. Because both CMRR and DMRR are usually very small, parasitic parameters can significantly affect them at high frequencies. Some designs are theoretically applicable; however due to parasitics, may not be good in practical designs.

For HF design, the conventional transformer T_1 and the conventional common choke L_1 shown in Fig. 9 should be avoided. The parasitic parameters in this noise separator are shown in Fig. 10. In Fig. 10, L_{K1}, L_{K2}, L_{K3} and L_{K4} are the leakage inductance between primary and secondary sides of the transformer. C_{W1} and C_{W2} are the winding capacitance between primary and secondary sides of the transformer. L_{K5} and L_{K6} are leakage inductance between two windings of the CM choke. Obviously the DM input impedance Z_{in} of the CM choke shown in Fig. 10 would no longer be real 100 Ω due to leakage inductance L_{K5} and L_{K6} at high frequencies. L_{K1}, L_{K2}, L_{K3} and L_{K4} also introduce extra impedances at high frequencies. As a result of these parasitics, the input impedances of the separator would deviate from real 50 Ω at high frequencies. The transformer would also no longer block CM noise at high frequencies due to winding capacitance C_{W1} and C_{W2}. The CMRR is therefore compromised. The transformer could be unbalanced at high frequencies due to parasitic parameters, which also degrades the CMRR and DMRR. In order to reduce leakage inductance, two windings of the transformer are twisted in paper [4]; however this increases winding capacitance so that CMRR is degraded.

For the noise separators in [6], [18], conventional transformers are used at outputs for impedance transformation [18]: 50 Ω–100 Ω and 50 Ω–25 Ω. These transformers have two disadvantages: first, the parasitics degrade separator HF performance; second, the output is 3-dB higher. Output should be redesigned to get rid of conventional transformers. The transmission line transformers [17], which have much better performance at high frequencies, should be used in noise separator design.

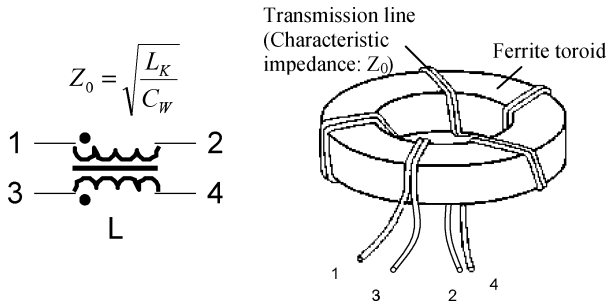

Fig. 11. Transmission line transformer.

IV. Developing a High Performance Noise Separator

In order to build a high performance noise separator, transmission line transformers [17] are employed in this paper. A transmission line transformer is constructed by winding a transmission line on a magnetic core such as a ferrite toroid. Fig. 11 shows the schematic and the typical structure of a transmission line transformer. In Fig. 11, two wires form a transmission line and are wound on a ferrite toroid. L is the CM inductance of transmission line, which is attributed to the high permeability of the ferrite toroid. The DM inductance L_{K} of the transmission line is factually the distributed leakage inductance of two CM inductance. C_{W} is the distributed winding capacitance between two wires. Ignoring the losses, it is well-known that the characteristic impedance Z_0 of the transmission line is given by

$$Z_0 = \sqrt{\frac{L_K}{C_W}}. \tag{27}$$

Z_0 can be determined through measurements using

$$Z_0 = \sqrt{Z_S Z_P} \tag{28}$$

where Z_{S} is the short-circuit impedance (with the other end of the transmission line short-circuited) and Z_{P} is the open-circuit impedance (with the other end of the transmission line open).

According to transmission line theory, if the characteristic impedance is equal to load impedance, the input impedance is equal to load impedance. The DM input impedances Z_{in1} and Z_{in2} of transmission line transformer shown in Fig. 12 are therefore equal to half of the load impedance. The output DM voltage is also equal to input DM voltage. The CM input impedance is very high because of CM inductance and HF losses. As a result the output CM voltage is very small.

These properties are important because the effects of the winding capacitance and the leakage inductance are cancelled so that DM input is transferred to the load without change. The negative effects of parasitics are factually excluded. It is a significant difference from the conventional CM choke shown in Fig. 10.

The transmission line transformer can also be connected to the style as shown in Fig. 13. In Fig. 13, the terminals 2 and 3 and load R_L are connected together. It can be proven that if

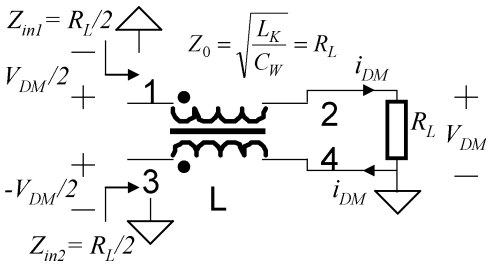

Fig. 12. Utilizing winding capacitance and leakage inductance to match DM load.

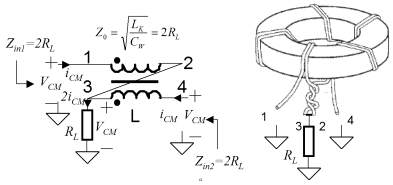

Fig. 13. Utilizing winding capacitance and leakage inductance to match CM load.

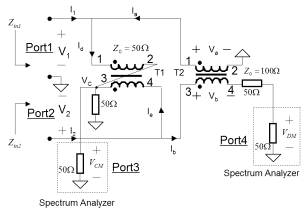

Fig. 14. Proposed noise separator.

the characteristic impedance of the transmission line is equal to $2R_L$, CM input impedances Z_{in1} and Z_{in2} are $2R_L$. The CM input is then added to the load without change. Because effects of the winding capacitance and the leakage inductance are cancelled, the negative effects of parasitics are excluded so that the design is better than the design in Fig. 10. Because two windings are in series for DM noise, the DM input impedance is very high. Because load is connected to the midpoint of two windings, the output due to DM inputs is zero.

A performance-improved noise separator shown in Fig. 14 is finally proposed based on the circuits in Figs. 12 and 13. In Fig. 14, transmission line transformer T1 is connected as in Fig. 13. It conducts CM noise, while blocks DM noise. T2 is connected as in Fig. 12. It conducts DM noise, while blocks CM noise. A 50 Ω resistor is in parallel with the input impedance of the spectrum analyzer at CM output port, and another 50 Ω resistor is in series with the input impedance of the spectrum analyzer at DM output port. Based on previous analysis, this simple design for outputs results in two benefits: 1) Real 50 Ω DM and CM input impedances occur without using conventional transformers at output to transform impedance. 2) Outputs are exact DM and CM noise voltages: no extra adjustment needed.

The following is the circuit analysis for Fig. 14 on output voltages and input impedances

$$\mathbf{V_b} = \mathbf{V_a} = \mathbf{V_1} \tag{29}$$

$$\mathbf{V}_{DM} = \frac{\mathbf{V_2} - \mathbf{V_1}}{2} \tag{30}$$

$$\mathbf{V}_{CM} = \mathbf{V_C} = \frac{\mathbf{V_2} + \mathbf{V_1}}{2}. \tag{31}$$

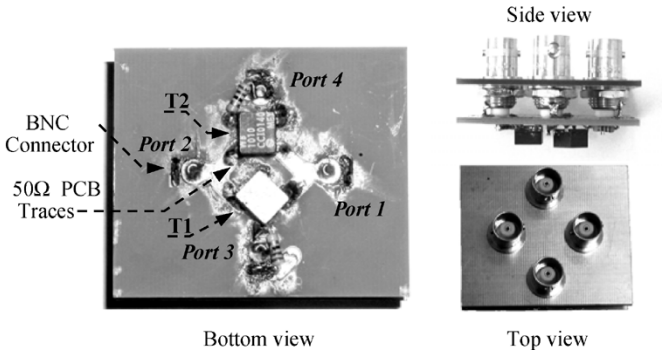

Fig. 15. Prototype of the proposed noise separator.

From (30) and (31), the separator outputs the exact DM and CM noise voltages. The input impedances are real 50 Ω, because

$$\mathbf{I_a} = \mathbf{I_b} = \frac{\mathbf{V_2} - \mathbf{V_1}}{100} \tag{32}$$

$$\mathbf{I_d} = \mathbf{I_e} = \frac{\mathbf{V_2} + \mathbf{V_1}}{100} \tag{33}$$

$$Z_{in1} = \frac{\mathbf{V_1}}{\mathbf{I_1}} = \frac{\mathbf{V_1}}{\mathbf{I_d} - \mathbf{I_a}} = 50\ \Omega \tag{34}$$

$$Z_{in2} = \frac{\mathbf{V_2}}{\mathbf{I_2}} = \frac{\mathbf{V_2}}{\mathbf{I_b} + \mathbf{I_e}} = 50\ \Omega. \tag{35}$$

In the design, the characteristic impedance should be 50 Ω for T1 and 100 Ω for T2. For convenience, commercial products (Coilcraft WB1010, inductance: 780 μH, 250 mA, ferrite toroid, Z_0 : 100 Ω) are used in the design. The magnetizing inductance of the transformer should be large enough to cover low end frequency. The length of winding wires should be as short as possible to reduce the effects of possible standing waves in the windings. The characteristic impedance of PCB traces is designed to 50 Ω because their parasitic inductance and capacitance may affect noise separator HF performance.

The prototype is shown in Fig. 15. Port1 and 2 are for inputs, port3 is for CM output and port4 is for DM output. In the design, in order to keep four ports an equal ground potential at high frequencies, four BNC connectors are mounted on one PCB and kept as close as possible.

The S-parameters of the prototype are measured using an HP 4195A network/spectrum analyzer. The oscillator level is set at 122 dBμV (Maximum level HP4195A can offer). For higher noise power measurement, two precision 50 Ω attenuators can be used before the noise separator. For EMI standard EN55022, the sweep range is from 150 kHz to 30 MHz (other EMI standards may specify different frequency ranges). When the DM noise separator is measured, the CM port is terminated by a 50 Ω termination and vice versa. Measurement results are shown in Figs. 16 and 17.

From Figs. 16 and 17, because the approximation conditions for (19)–(24) are satisfied, the input impedances are therefore independent from noise source impedances and are calculated using (19) and (20). CMTR and DMTR, CMRR and DMRR are calculated using (21)–(24). All of them are shown from Figs. 18–20. Fig. 18 shows that the input impedances are between 48.4 Ω and 50.8 Ω; the phases are between 0.3° and 3.3°. They are very near a real 50 Ω. From Figs. 19 and 20, the

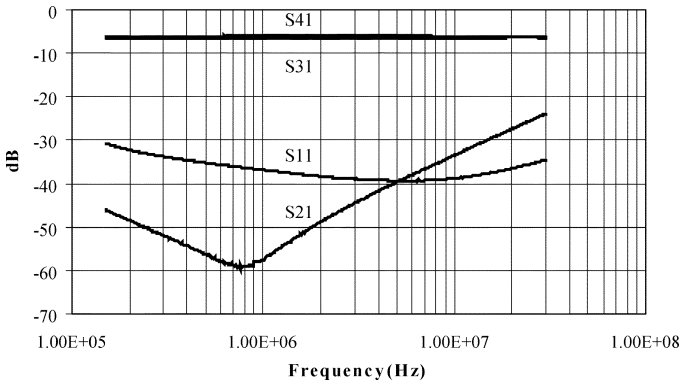

Fig. 16. Measured S-parameters of the prototype.

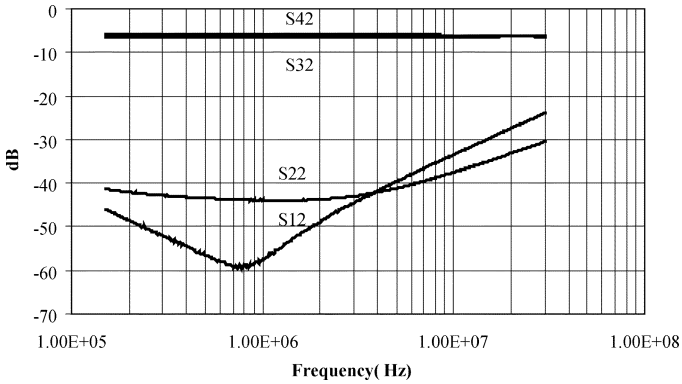

Fig. 17. Measured S-parameters of the prototype.

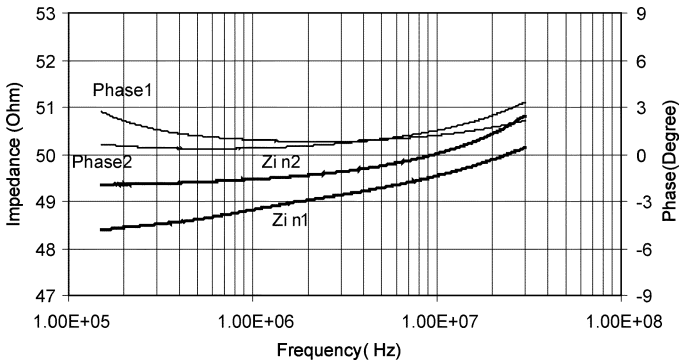

Fig. 18. Input impedances of the prototype.

$\mathrm{DMRR} < -65$ dB and the $\mathrm{CMRR} < -51$ dB, so the leakage between DM and CM is very small. Transmission ratios DMTR and CMTR range from 0.1 dB to -0.5 dB. The prototype satisfies all the requirements and achieves DM and CM noise separators in one circuit.

Based on all these analyzes and measurements, the proposed noise separator has the following advantages.

1) Input impedances are always real 50 Ω and are independent from source impedances.
2) Outputs are exact DM and CM noise voltages.
3) DM and CM are simultaneously measured using the same circuit.
4) DMRR and CMRR are very good.

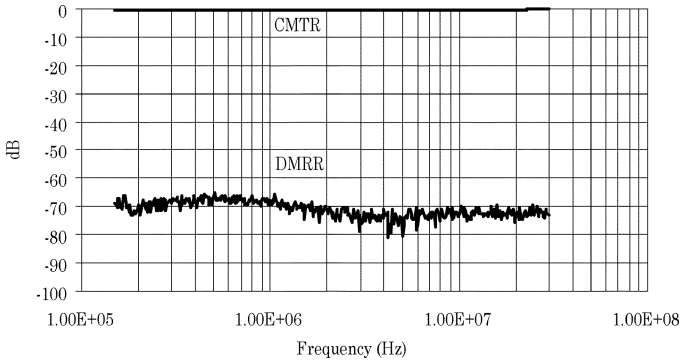

Fig. 19. DMRR and CMTR of the prototype.

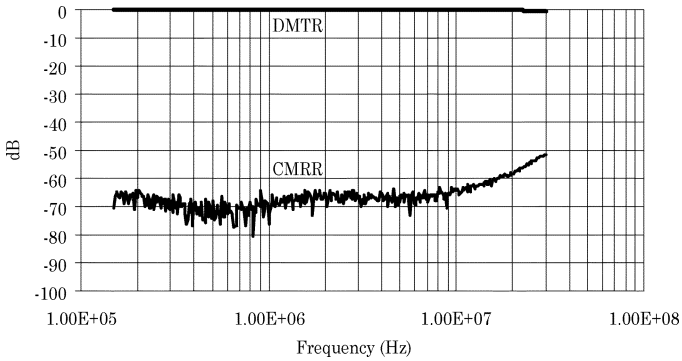

Fig. 20. CMRR and DMTR of the prototype.

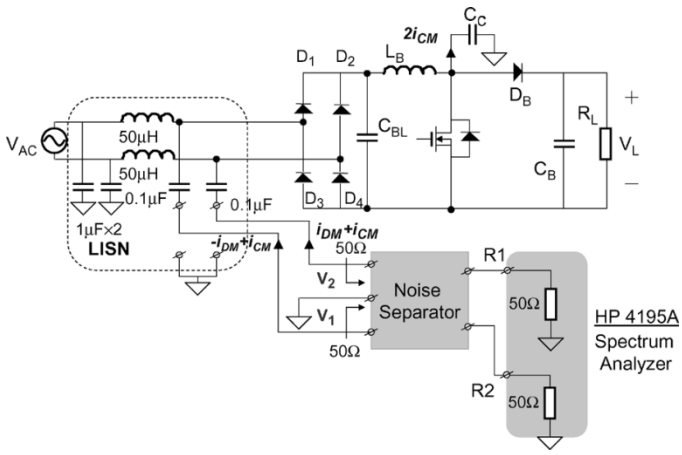

Fig. 21. Conducted EMI measurement setup for a 1.1-kW PFC converter.

V. Noise Measurement Results

The prototype was finally used for the noise measurement of a 1.1-kW PFC converter. The PFC converter has a circuit topology similar to that shown in Fig. 2 and a switching frequency of 67 kHz. The measurement setup is shown in Fig. 21. An HP 4195A network/spectrum analyzer is used in the measurement. Because the HP 4195A has four input ports for spectrum measurement, port3 and port4 of the prototype were connected to input ports R1 and R2 of the HP 4195A, respectively, through 50 Ω coaxial cables. In the measurement, DM and CM noise can be measured separately just by selecting the input port between R1 and R2 through the panel of HP 4195A or the connected computer. There is no need to replace the noise separator or shut off the converter, which is very convenient.

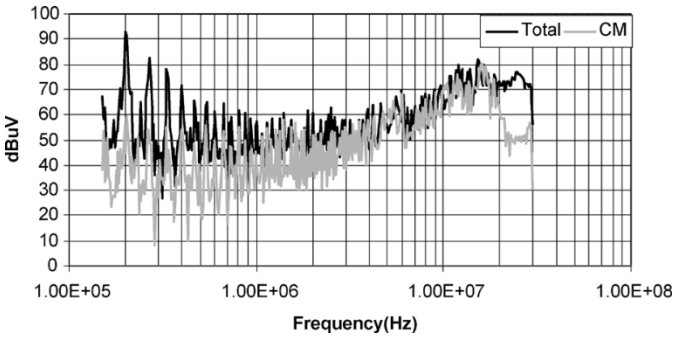

Fig. 22. Total noise and CM noise when heat-sink is ungrounded.

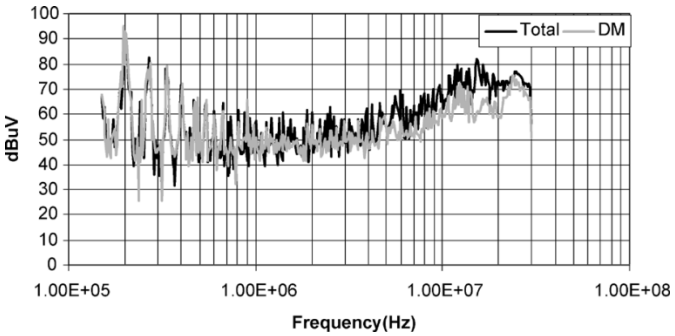

Fig. 23. Total noise and DM noise when heat-sink is ungrounded.

For this PFC converter, diode $\mathrm{D_B}$ and the MOSFET are mounted on one heat-sink. Experiments are carried out for two cases. In the first case, the heat-sink of the converter is not grounded; therefore the parasitic capacitance $\mathrm{C_C}$ in Fig. 21 is small. In the second case, the heat-sink is grounded, so $\mathrm{C_C}$ is larger. It is expected that the CM noise in the second case will be much larger, and DM noise will be almost same due to balance capacitor $\mathrm{C_{BL}}$. Figs. 22 and 23 show measured CM, DM, and total noise when the heat-sink is ungrounded. It shows that for this case, total noise is determined by DM noise when the frequency is below 1 MHz and above 20 MHz; meanwhile CM noise is dominant from 1 MHz to 20 MHz.

Figs. 24 and 25 show results after the heat-sink is connected to the ground. Once the heat-sink is grounded, CM noise is dominant in almost the entire frequency range (150 kHz–30 MHz) because of the larger $\mathrm{C_C}$. DM noise is almost unchanged. This proves the good performance of the prototype.

Based on the preceding S-parameters and noise measurements, the prototype can correctly and accurately separate DM and CM noise; thus it is a powerful tool for EMI noise diagnosis.

VI. Conclusion

In this paper, both ideal and practical noise separators are initially characterized using S-parameters. Based on these models, the methods and equations used to correctly and accurately evaluate noise separators are specified and developed. Existing noise separators are investigated one by one according to developed methods and equations. It is found that most existing noise separators offer neither real 50 Ω input impedance nor exact noise separation. A performance-improved noise separator is then proposed with parasitic cancellation. The prototype is evaluated using the developed methods. Experiments verify that the proposed noise separator satisfies all requirements and that it shows very good performance.

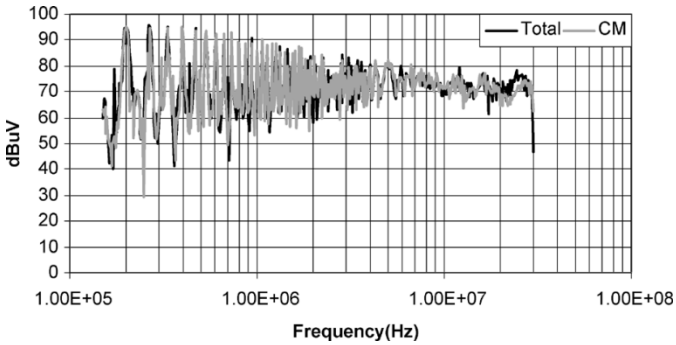

Fig. 24. Total noise and CM noise after heat-sink is grounded.

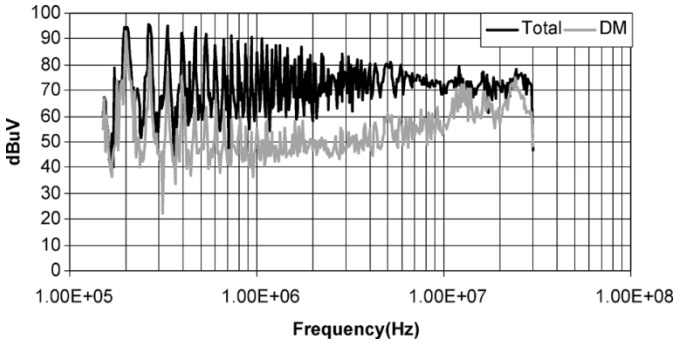

Fig. 25. Total noise and DM noise after heat-sink is grounded.

References

[1] C. R. Paul and K. B. Hardin, "Diagnosis and reduction of conducted noise emissions," *IEEE Trans. Electromagn. Compat.*, vol. 30, no. 4, pp. 553–560, Nov. 1988.

[2] H.-L. Su and K.-H. Lin, "Computer-aided design of power line filters with a low cost common and differential-mode noise diagnostic circuit," in *Proc. IEEE Electromagnetic Compatibility Int. Symp.*, Montreal, QC, Canada, Aug. 13–17, 2001, pp. 511–516.

[3] M. C. Caponet, F. Profumo, L. Ferraris, A. Bertoz, and D. Marzella, "Common and differential mode noise separation: comparison of two different approaches," in *Proc. IEEE Power Electronics Specialist Conf.*, Vancouver, BC, Canada, Jun. 17–21, 2001, pp. 1383–1388.

[4] M. C. Caponet and F. Profumo, "Devices for the separation of the common and differential mode noise: design and realization," in *Proc. IEEE Applied Power Electronics Conf. Expo*, Dallas, TX, Mar. 10–14, 2002, pp. 100–105.

[5] M. J. Nave, "A novel differential mode rejection network for conducted emissions diagnostics," in *Proc. IEEE Electromagnetic Compatibility Nat. Symp.*, Denver, CO, May 23–25, 1989, pp. 223–227.

[6] G. Ting, D. Y. Chen, and F. C. Lee, "Separation of the common-mode and differential-mode conducted EMI noise," *IEEE Trans. Power Electron.*, vol. 11, no. 3, pp. 480–488, May 1996.

[7] S. K. Yak and N. C. Sum, "Diagnosis of conducted interference with discrimination network," in *Proc. IEEE Power Electronics Drive Systems Int. Conf.*, Singapore, Feb. 21–24, 1995, pp. 433–437.

[8] Y.-K. Lo, H.-J. Chiu, and T.-H. Song, "A software-based CM and DM measurement system for the conducted EMI," *IEEE Trans. Ind. Electron.*, vol. 47, no. 4, pp. 977–978, Aug. 2000.

[9] M. J. Nave, *Power Line Filter Design for Switched-Mode Power Supply*. New York: Van Nostrand Reinhild, 1991.

[10] D. M. Pozar, *Microwave Engineering*. New York: Wiley, 1998.

[11] N. Balabanian and T. Bickart, *Linear Network Theory: Analysis, Properties, Design and Synthesis*. New York: Matrix, 1981.

[12] W. Medley, *Microwave and RF Circuits: Analysis, Synthesis, and Design*. Boston, MA: Artech House, 1993.

[13] Agilent AN154 S-Parameters Design Application Note, Agilent Technologies, 2000.

[14] W. Zhang, W. Dongbing, D. Y. Chen, and D. Sable, "A new method to characterize EMI filters," in *Proc. IEEE Applied Power Electronics Conf. Expo*, Anaheim, CA, Feb. 15–19, 1998, pp. 929–933.

[15] R. Anderson, Test and Measurement Application Note 95-1 S-Parameters Techniques, Hewlett-Packard, 1997.

[16] A. Nagel and R. W. De Donker, "Separating common mode and differential mode noise in EMI measurements," in *Proc. EPE'99 Conf.*, Lousanne, France, 1999, pp. 1–8.
[17] J. Sevick, *Transmission Line Transformers*. New York: American Radio Relay League, 1987.
[18] G. Ting, "Separation of the common-mode and the differential-mode conducted electromagnetic interference noise," M.S. thesis, Virginia Tech, Blacksburg, VA, 1994.

Shuo Wang (S'03) received the B.S.E.E degree from Southwest Jiaotong University, Chengdu, China, in 1994, the M.S.E.E degree from Zhejiang University, Hangzhou, China, in 1997, and is currently pursuing the Ph.D. degree at the Center for Power Electronics Systems (CPES), Virginia Polytechnic Institute and State University, Blacksburg.

From 1997 to 1999, he was with ZTE Telecommunication Corporation, Shenzhen, China, where he was a Senior R&D Engineer and responsible for the development and support of the power supply for wireless products. In 2000, he worked at UTstarcom Telecommunication Corporation, Hangzhou, China, where he was responsible for the development and support of the optical access networks. He has one U.S. patent pending.

Mr. Wang received the Excellent R&D Engineer Award in 1998.

Fred C. Lee (S'72–M'74–SM'87–F'90) received the B.S. degree in electrical engineering from the National Cheng Kung University, Taiwan, R.O.C., in 1968 and the M.S. and Ph.D. degrees in electrical engineering from Duke University, Durham, NC, in 1971 and 1974, respectively.

He is a University Distinguished Professor with Virginia Polytechnic Institute and State University (Virginia Tech), Blacksburg, and prior to that he was the Lewis A. Hester Chair of Engineering at Virginia Tech. He directs the Center for Power Electronics Systems (CPES), a National Science Foundation engineering research center whose participants include five universities and over 100 corporations. In addition to Virginia Tech, participating CPES universities are the University of Wisconsin-Madison, Rensselaer Polytechnic Institute, North Carolina A&T State University, and the University of Puerto Rico-Mayaguez. He is also the Founder and Director of the Virginia Power Electronics Center (VPEC), one of the largest university-based power electronics research centers in the country. VPEC's Industry-University Partnership Program provides an effective mechanism for technology transfer, and an opportunity for industries to profit from VPEC's research results. VPEC's programs have been able to attract world-renowned faculty and visiting professors to Virginia Tech who, in turn, attract an excellent cadre of undergraduate and graduate students. Total sponsored research funding secured by him over the last 20 years exceeds $35 million. His research interests include high-frequency power conversion, distributed power systems, space power systems, power factor correction techniques, electronics packaging, high-frequency magnetics, device characterization, and modeling and control of converters. He holds 30 U.S. patents, and has published over 175 journal articles in refereed journals and more than 400 technical papers in conference proceedings.

Dr. Lee received the Society of Automotive Engineering's Ralph R. Teeter Education Award (1985), Virginia Tech's Alumni Award for Research Excellence (1990), and its College of Engineering Dean's Award for Excellence in Research (1997), in 1989, the William E. Newell Power Electronics Award, the highest award presented by the IEEE Power Electronics Society for outstanding achievement in the power electronics discipline, the Power Conversion and Intelligent Motion Award for Leadership in Power Electronics Education (1990), the Arthur E. Fury Award for Leadership and Innovation in Advancing Power Electronic Systems Technology (1998), the IEEE Millennium Medal, and honorary professorships from Shanghai University of Technology, Shanghai Railroad and Technology Institute, Nanjing Aeronautical Institute, Zhejiang University, and Tsinghua University. He is an active member in the professional community of power electronics engineers. He chaired the 1995 International Conference on Power Electronics and Drives Systems, which took place in Singapore, and co-chaired the 1994 International Power Electronics and Motion Control Conference, held in Beijing. During 1993-1994, he served as President of the IEEE Power Electronics Society and, before that, as Program Chair and then Conference Chair of IEEE-sponsored power electronics specialist conferences.

Willem Gerhardus Odendaal (M'98) was born in South Africa in 1969. He received the B.Eng., M.Eng., and D.Eng. degrees in electrical and electronics engineering from Rand Arikaans University, Johannesburg, South Africa, in 1992, 1995, and 1997, respectively.

He spent one year in a post-doctoral position under two fellowships at the Virginia Power Electronics Center, Virginia Polytechnic Institute and State University (Virginia Tech), Blacksburg, before joining Philips Research North America, New York, NY, as Senior Member of Research Staff. Since Fall 2001, he has been Assistant Professor in the Bradley Department of Electrical and Computer Engineering, Virginia Tech, as well as a faculty member of the NSF Engineering Research Center for Power Electronics Systems, (or CPES). His research interests include electromagnetic and thermodynamic energy processing and packaging of power electronic circuits.

Dr. Odendaal is Chairman of the Power Electronics Devices and Components Committee, IEEE Industry Applications Society.